How to cite: *Angew. Chem. Int. Ed.* **2022,** *61,* e202206108
International Edition: doi.org/10.1002/anie.202206108
German Edition: doi.org/10.1002/ange.202206108

Supported Photocatalysts

Optimizing Pt Electronic States through Formation of a Schottky Junction on Non-reducible Metal–Organic Frameworks for Enhanced Photocatalysis

*Zi-Xuan Sun, Kang Sun, Ming-Liang Gao, Önder Metin, and Hai-Long Jiang**

Abstract: Charge transfer between metal sites and supports is crucial for catalysis. Redox-inert supports are usually unfavorable due to their less electronic interaction with metal sites, which, we demonstrate, is not always correct. Herein, three metal–organic frameworks (MOFs) are chosen to mimic inert or active supports for Pt nanoparticles (NPs) and the photocatalysis is studied. Results demonstrate the formation of a Schottky junction between Pt and the MOFs, leading to the electron-donation effect of the MOFs. Under light irradiation, both the MOF electron-donation effect and Pt interband excitation dominate the Pt electron density. Compared with the "active" UiO-66 and MIL-125 supports, Pt NPs on the "inert" ZIF-8 exhibit higher electron density due to the higher Schottky barrier, resulting in superior photocatalytic activity. This work optimizes metal catalysts with non-reducible supports, and promotes the understanding of the relationship between the metal–support interaction and photocatalysis.

Introduction

Metal nanoparticles (NPs) have been recognized to be the most important active sites in heterogeneous catalysis and have found applications in various industrial chemical transformations.[1] It is well established that reasonably small metal NPs are favorable to the activity. To retard the aggregation arising from their high surface energy, the dispersion or stabilization of metal NPs by diverse supports, such as metal oxides, porous matrices, have been intensively studied.[2] The interaction between the support and metal NPs is able to modulate the electronic properties of the metal and therefore greatly influences the catalysis.[3] For the most studied oxide supports, they are usually classified into active and inert supports. The active supports refer to the reducible metal oxides, including TiO_2, Fe_2O_3 and ZrO_2, etc. The redox-active metals involved in the active supports can lead to electron transfer with the metal NPs, which modulates the electronic state of metal active sites and therefore improves the catalytic performance.[3b,d,f] In contrast, inert supports, such as SiO_2 and MgO, featuring redox-inert species, have little interaction with metal NPs, which is unfavorable to catalysis.[4]

Similar to thermal catalysis, supported metal NPs are a type of important photocatalysts.[5] The current studies on these photocatalysts are mostly related to the regulation of metal NPs, for example, adjusting the morphologies and metal sizes or introducing a second component.[5b,c] There have been very rare reports on how the metal–support interaction affects photocatalysis. Halas et al. reported the superior activity of Au/SiO_2 to Au/TiO_2 in the photocatalytic H_2 dissociation reaction, which is possibly the only example of promoted catalysis with an inert support.[6] However, the function of SiO_2 in that work was blocking hot electrons due to its insulator property. The regulation of metal electronic state and the corresponding understanding of the metal–support interaction for photocatalysis have not yet been achieved. Therefore, it remains extremely rare yet necessary and highly desired to develop suitable model supports that help to gain insight into the role of metal–support electron transfer in photocatalysis.

In addition to the traditional metal oxides, different porous supports have been developed.[2b,d,e] Amongst the porous solids, metal–organic frameworks (MOFs),[7] constructed by metal (clusters) and organic linkers, possessing atomically precise and tailored structures as well as high porosity, have been recognized to be very promising supports for metal NPs, being an ideal platform to understand the metal–support interaction.[8] Notably, most MOFs behave like semiconductors with the conductive band (CB, also called lowest unoccupied molecular orbital, LUMO) mainly contributed by metal clusters and the valence band (VB, also called highest occupied molecular orbital, HOMO) mainly contributed by organic linkers, presenting similarity with metal oxide supports.[9] Meanwhile, the spectral absorption range of MOFs is highly tunable from ultraviolet (UV) to near-infrared (NIR) regions, capable of avoiding the interference with the optical response of metal NPs. On consideration of the weaker chemisorption states of reactants on classical plasmonic metals (Au, Ag and Cu)

[*] Z.-X. Sun, K. Sun, Dr. M.-L. Gao, Prof. Dr. H.-L. Jiang
Department of Chemistry, University of Science and Technology of China
Hefei, Anhui 230026 (P.R. China)
E-mail: jianglab@ustc.edu.cn
Homepage: http://staff.ustc.edu.cn/~jianglab/
Prof. Dr. Ö. Metin
Department of Chemistry, College of Sciences, Koç University
Istanbul 34450 (Turkey)

due to their full *d*-orbits and low *d*-band centers,[10] the interband excitation of Pt NPs can be adopted to harvest visible light, favorable to chemisorption and activation of substrates.[11] It is worth noting that, although there have been some reports on the interband excitation,[12] as far as we know, it remains barely investigated how the metal–support charge transfer induced by interband excitation affects the photocatalysis.

In this work, three representative MOFs, namely ZIF-8, UiO-66, and MIL-125, without visible-light response were chosen to stabilize small-size Pt NPs to afford Pt/MOF. The metals constituted for the MOFs are Zn^{II}, Zr^{IV} and Ti^{IV}, respectively, giving rise to the non-reducible support properties of ZIF-8 and reducible supports properties of UiO-66 and MIL-125, due to the difficulty of reducing d^{10} Zn^{II} and relatively smaller barrier to reduce Zr^{IV} and Ti^{IV}. Under the Pt interband excitation wavelength of 450 nm, photocatalytic aerobic oxidative coupling of benzylamine has been conducted to investigate the influence of metal–support interactions on photocatalysis. It is surprising to find that the photocatalytic activity follows the order of Pt/ZIF-8 > Pt/UiO-66 > Pt/MIL-125. Spectral and energy band studies indicate the existence of two-step electron transfer, including the MOF electron donation originated from metal–support contact and inverse electron injection from Pt interband excitation. The two processes can be largely regulated by adopting MOFs with different energy band structures, significantly affecting the Pt electronic states. As a result, the highest Pt electron density is observed when Pt is supported on ZIF-8, leading to the best photocatalytic activity. To the best of our knowledge, this is the first report on optimized Pt activity with the inert support, surpassing the active supports, in photocatalysis.

Results and Discussion

The ZIF-8, UiO-66 and MIL-125,[13] were synthesized by the documented hydrothermal methods (Figure S1 in the Supporting Information). Their phase purity and crystallinity were confirmed by powder X-ray diffraction (XRD) (Figure S2). Thermogravimetric analysis supports the complete removal of unreacted linkers of ZIF-8 (Figure S3). Scanning electron microscopy (SEM) images indicate their very good dispersity and shape with sizes of 0.1–1 μm (Figure 1a, S4a and S5a). Upon immobilization of Pt NPs to the MOFs by impregnating H_2PtCl_6 and subsequent H_2 reduction, the corresponding catalysts of Pt/ZIF-8, Pt/UiO-66 and Pt/MIL-125 were obtained, where Pt loadings (~1.8 wt%) are similar as determined by inductively coupled plasma atomic emission spectrometry (ICP-AES) (Table S1). Transmission electron microscopy (TEM) images display that Pt NPs are dispersed uniformly on the MOF surface with similar Pt sizes of ~3.5 nm, exposing Pt (111) plane with a lattice fringe spacing of 0.226 nm (Figure 1b,c, S4b, S4c, S5b and S5c). Nitrogen sorption isotherms reveal the similar porous features before and after the introduction of Pt NPs, while the slightly decreased BET surface areas and total pore volumes compared with the corresponding parent MOFs might be attributed to the Pt mass occupation (Figure S4d, S5d, S6 and S7). UV-vis spectra indicate that the MOFs are optically transparent in the visible light region. After introducing Pt NPs, all composites exhibit enhanced absorption in 380–780 nm contributed by the interband transition of Pt (Figure 1d and S8).[11a,14]

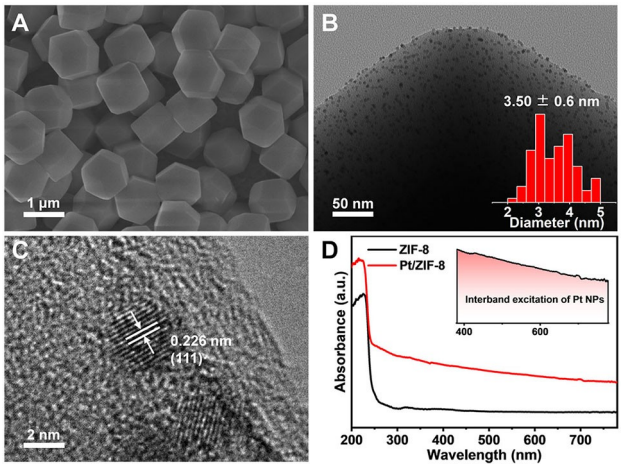

Figure 1. a) SEM image for ZIF-8. b) TEM (inset: size distribution of Pt NPs), and c) high-resolution TEM images for Pt/ZIF-8. d) UV-vis spectra for ZIF-8 and Pt/ZIF-8 (inset: differential spectrum of absorbance of Pt/ZIF-8 and ZIF-8 in 380–780 nm).

The energy band structures of MOFs are decided by the Tauc and Mott–Schottky plots (Figure S9–S11). The positive slope of Mott–Schottky plots suggests that all MOFs are *n*-type semiconductors with electrons as the majority carriers.[15] Compared with the parent MOFs, the upwards flat-band positions of Pt/MOFs indicate the formation of Schottky junction at the interface of Pt and the MOFs (Figure S9b, S10b, S11b and S12–S14), in line with the weakened photoluminescence intensity upon deposition of Pt onto the MOFs (Figure S15–S17).[16] As a control, Pt/SiO_2 was synthesized and it is well accepted that no metal–support electron transfer is involved in Pt/SiO_2 due to the insulator characteristics of SiO_2.[17] The loading amount and size distribution of Pt in Pt/SiO_2 are similar to those in the Pt/MOFs (Table S2 and Figure S18). X-ray photoelectron spectroscopy (XPS) and the diffuse reflectance infrared Fourier transform of CO adsorption (CO-DRIFT) have been conducted to evaluate the electronic states of Pt in the Pt/MOFs and Pt/SiO_2 (Figure 2a and b). The XPS binding energy of Pt 4f on different supports gives the trend of Pt/SiO_2 > Pt/MIL-125 > Pt/UiO-66 > Pt/ZIF-8, indicating the most electron-deficient Pt on SiO_2 while the most electron-rich Pt on ZIF-8. The CO chemisorption on Pt is in line with the above XPS results, supporting that the Pt electron density follows Pt/ZIF-8 > Pt/UiO-66 > Pt/MIL-125 > Pt/SiO_2. The discriminative Pt electron density can be attributed to the different LUMO levels and electron donation effect of these *n*-type semiconductor-like MOFs. ZIF-8 donates more electrons to Pt NPs than UiO-66 and MIL-125 based on the formation mechanism of the Schottky junction, which we will elaborate on in the following parts.

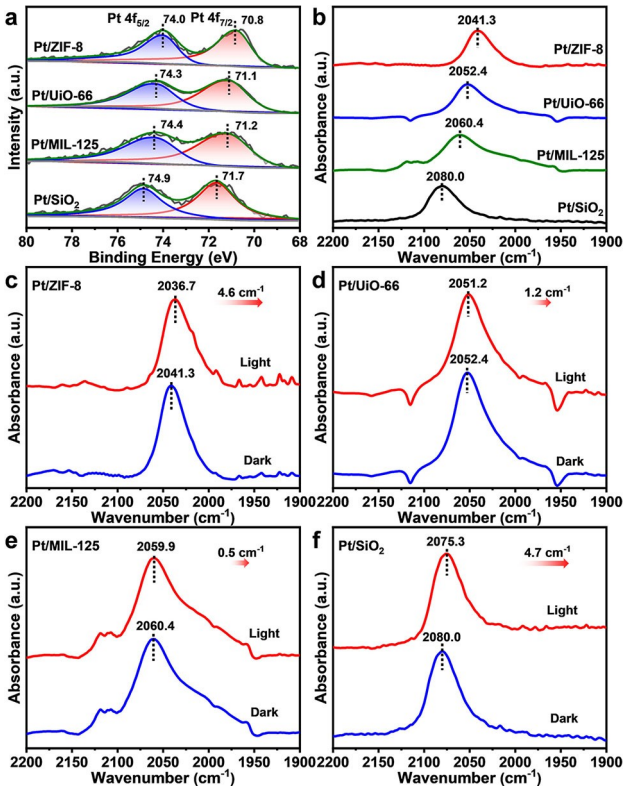

Figure 2. a) XPS spectra of Pt 4f, and b) DRIFT spectra of CO adsorption on Pt in the dark for Pt/ZIF-8, Pt/UiO-66, Pt/MIL-125, and Pt/SiO_2. c)–f) DRIFT spectra of CO adsorption on Pt in the dark and under light irradiation for c) Pt/ZIF-8, d) Pt/UiO-66, e) Pt/MIL-125, and f) Pt/SiO_2.

Furthermore, *in situ* CO-DRIFT spectra under 450 nm light irradiation have also been carried out to examine the interband-excited electrons of Pt NPs (Figure 2c–f). While both spectra of Pt/ZIF-8 and Pt/SiO_2 exhibit similar red shifts (~5 cm^{-1}) compared with those in the dark, Pt/UiO-66 and Pt/MIL-125 present much smaller red shifts of 1.2 cm^{-1} and 0.5 cm^{-1}, respectively. It is assumed that the photo-excited energetic electrons of Pt NPs are injected into the $2\pi^*$ orbitals of CO (electron backdonation), resulting in a stronger Pt–CO adsorption and the lower wavenumber under light irradiation. Given the observed results in the XPS and CO-DRIFT spectra (Figure 2), the electronic state of Pt active sites can be well modulated with different supports, which would give rise to distinctly different performances in photocatalysis.

Inspired by the above results, photocatalytic oxidative coupling of benzylamine, an essential reaction in the pharmacy and fine chemical industry,[18] has been conducted to verify the photocatalytic performance of Pt supported on the different MOFs. To eliminate the interference of MOF excitation, 450 nm blue light is chosen for the photocatalytic reaction. As shown in Figure 3a, the Pt/MIL-125 gives only 5.5 % conversion of benzylamine. Changing the support to UiO-66, the conversion is slightly improved to 12.2 %. Strikingly, the conversion of benzylamine by using Pt/ZIF-8 with an inert support is elevated to 99.7 % with 99.1 %

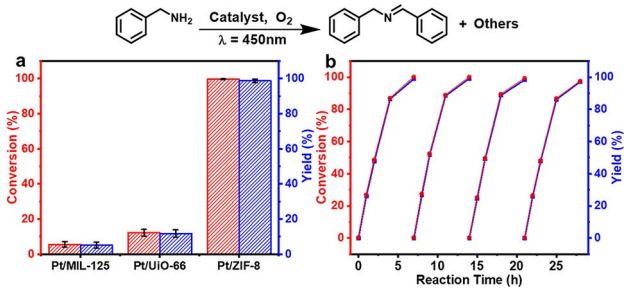

Figure 3. a) Catalytic conversion and yield of photocatalytic oxidative coupling of benzylamine over the Pt/MOF composites (the error bars represent the relative deviation obtained from parallel experiments). b) The consecutive four runs of photocatalytic reaction over Pt/ZIF-8. The red data points represent conversion and the blue data points represent the yield. The conversion is not exactly equal to the yield.

selectivity to the target product of N-benzylidenebenzylamine, unambiguously demonstrating the remarkable influence of the MOF supports on the activity. The target product is confirmed by gas chromatography–mass spectrometry (GC-MS) (Figure S19). The time-dependent conversion curve reveals that the kinetics of the catalytic process by Pt/ZIF-8 can be fitted to the first-order reaction (Figure S20). Photocatalytic reaction rates of Pt/UiO-66 and Pt/MIL-125 remain nearly unchanged when the time length is prolonged to 24 h (Figure S20a). Additional experiments indicate that both the support basicity and substrate adsorption do not play a critical role in the superior activity of Pt/ZIF-8 (Table S3, S4).

Control experiments have been conducted to decode the roles of each component in the reaction (Table 1). The target product is nearly undetectable in the absence of the Pt/MOF, O_2, or light irradiation (entries 2, 3, and 5). The conversion decreases in air instead of O_2 (entry 4), indicating that O_2 is indispensable for this reaction. The MOFs exhibit negligible conversion, suggesting Pt NPs are the active sites (entries 6–8). Furthermore, the polyvinylpyrrolidone (PVP) protected Pt_{PVP} NPs were synthesized to perform the photocatalytic reaction (Figure S21a). They unfortunately show very low activity (entry 9), possibly resulting from the hindering effect of PVP and/or the low stability and the absence of Pt/support interface (Figure S21b). The physical mixture of Pt_{PVP} NPs with ZIF-8 slightly increases the conversion (Table 1, entry 10 and Figure S21c, d). These results clearly highlight the advantages of supporting Pt NPs onto the MOFs.

The stability of the best-performance Pt/ZIF-8 has been further examined by performing a recycling test, which manifests that its activity and selectivity can be well retained in the four consecutive photocatalytic runs (Figure 3b), suggesting the high stability of Pt/ZIF-8. Powder XRD patterns demonstrate the structural integrity and crystallinity of the MOFs are maintained, and the Pt sizes and loading amounts are almost not changed after the reaction, further illustrating the great stabilization effect of the MOFs (Figure S22, S23 and Table S5). In addition, the photocatalytic activity of oxidative coupling of various amines over Pt/ZIF-

Table 1: Photocatalytic results for oxidative coupling of benzylamine under different conditions.

Entry	Catalyst	O_2	Light	Conv. [%]	Yield [%]
1[a]	Pt/ZIF-8	+	+	99.6	98.7
2	/	+	+	1.58	1.4
3	Pt/ZIF-8	N_2	+	–	–
4	Pt/ZIF-8	Air	+	85.9	85.6
5	Pt/ZIF-8	+	–	1.3	1.1
6	ZIF-8	+	+	3.7	3.5
7	UiO-66	+	+	3.0	3.0
8	MIL-125	+	+	4.0	3.3
9[b]	Pt_{PVP} NPs	+	+	20.1	16.8
10[c]	Pt_{PVP} NPs + ZIF-8	+	+	26.8	25.3

[a] Standard reaction conditions: 1 mL anhydrous DMF, 10 mg catalyst, 11 μL benzylamine, 450 nm LED, O_2 balloon, 7 h. The conversion and yield were determined by GC analysis, and *n*-dodecane was used as the internal standard. [b] The 0.18 mg Pt_{PVP} NPs was dissolved in 0.18 mL anhydrous DMF, then the mixed solution was added into 0.82 mL anhydrous DMF, while fixing other reaction parameters. [c] The 0.18 mg Pt_{PVP} NPs and 9.8 mg ZIF-8 were dissolved in 0.18 mL anhydrous DMF, then the mixed solution was added into 0.82 mL anhydrous DMF, while fixing other reaction parameters.

8 has been examined (Table S6). To our delight, a variety of amine substrates can be well tolerated for the oxidative coupling. Benzylamines substituted with electron-donating groups (–OCH_3, –CH_3, –F) and electron-withdrawing groups (–Cl, –CF_3) are all reacted with high conversion and yield (Table S6, entries 1–6). The slightly higher reaction rates of *p*-methoxyl benzylamine than *m*-methoxyl benzylamine might be ascribed to the steric effect. While heterocyclic amines containing N, O and S atoms usually poison metal sites, they can also participate in the reaction with satisfied conversion and yield (Table S6, entries 7–9). When the substrates are extended to cyclic and aliphatic amines, Pt/ZIF-8 is also able to convert them to corresponding imines (Table S7), reflecting the good compatibility and tolerance of this photocatalyst.

To gain insight into the relationship between metal–support electron transfer and photocatalytic activity, the photocatalytic mechanism is further investigated. By replacing light irradiation with heating, low activity is observed in the range of 15–60 °C (Figure 4a). Moreover, the catalytic activity of Pt/ZIF-8 is linearly dependent on the light intensity (Figure S24).[19] When triethylamine (TEA, hole scavenger) or $AgNO_3$ (electron scavenger) is added to the reaction system, the conversion significantly reduces (Figure 4b), further supporting the mechanism of energetic charge carriers mediated process rather than photothermal effect. Given that oxygen is indispensable in the reaction as evidenced above (Table 1), it is necessary to figure out the specific reactive oxygen species (ROS) involved in the reaction based on quenching experiments by adding different scavengers (Figure 4b). Typically, the activity dramatically reduces by introducing only *p*-benzoquinone (*p*BQ, $O_2^{\bullet-}$ scavenger), while *t*-butanol (TBA, $^{\bullet}OH$ scavenger) and 2-methylfuran (sylvan, $^1O_2$ scavenger) exhibit negligible quenching effect, indicating $O_2^{\bullet-}$ is the crucial ROS in this photocatalytic system. Moreover, the electron paramagnetic resonance (EPR) signal with the addition of $O_2^{\bullet-}$ trapping agent DMPO displays the typical signal of DMPO-$O_2^{\bullet-}$ with the signal intensity sequence of Pt/ZIF-8 > Pt/UiO-66 ≈ Pt/MIL-125, in consistent with the activity order, further

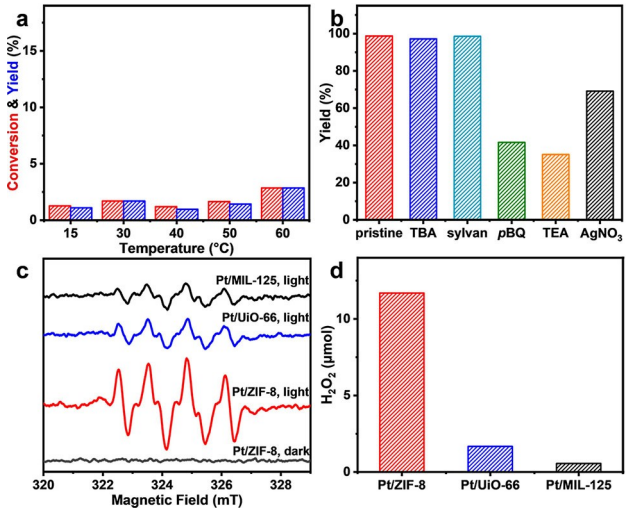

Figure 4. a) The photocatalytic performance of Pt/ZIF-8 at different temperatures in the dark. b) Yield of target product using Pt/ZIF-8 in the absence (pristine) or presence of different scavengers (50 mM). c) EPR spectra for the $O_2^{\bullet-}$ detection in the presence of different photocatalysts in the dark or under light irradiation. d) The H_2O_2 amounts produced in the photocatalytic reaction with different Pt/MOF composites.

proving the generation of superoxide radicals (Figure 4c). Then, the mechanism of oxidative coupling of benzylamine involving $O_2^{\bullet-}$ is investigated. The $O_2^{\bullet-}$ tends to induce the nucleophilic attack of the positively charged species and react with protons to form H_2O_2.[20] The negative slope of the Hammett plot indicates the existence of positively charged intermediates, probably $PhCH_2NH_2^{\bullet+}$ generated from benzylamine oxidized by photogenerated hot holes of Pt NPs (Figure S25).[21] Moreover, the amounts of H_2O_2 are detected by the iodometry method (Figure S26). Results illustrate that the produced H_2O_2 amounts follow the same sequence as those of $O_2^{\bullet-}$ (Figure 4d). Meanwhile, the other byproduct, NH_3, can be proved by the indophenol blue method (Figure S27). With these experimental results, the corresponding photocatalytic reaction mechanism can be

proposed (Figure S28), in which the $O_2^{\bullet-}$ generated from photogenerated electrons further acquires protons from $PhCH_2NH_2^{\bullet+}$ to release H_2O_2 and N-benzylideneamine that couples with another benzylamine to afford the imine product.

According to the regulated Pt electronic states proved by XPS and CO-DRIFT spectra (in the dark and light irradiation) above (Figure 2), as well as the photocatalytic mechanism, it is assumed that the existence of two-step charge transfer processes, including electron donation from the MOFs to Pt (upon contact, in the dark) and the migration of photo-excited electrons of Pt (upon light irradiation) (Figure 5a), would have an influence on $O_2^{\bullet-}$ production and the corresponding photocatalytic activity. The two processes are originated from the Schottky junction formation and Pt interband excitation under light conditions, respectively. To validate these two processes, Pt/SiO_2 is employed as a reference for the photocatalytic oxidative benzylamine coupling reaction. The Pt in Pt/SiO_2 presents the lowest electron density owing to the insulating property of SiO_2, as noted above (Figure 2a and b). Despite the leaching of a part of Pt (Table S2), the 55 % photocatalytic conversion over Pt/SiO_2 is much higher than that of Pt/UiO-66 and Pt/MIL-125 (Figure S29). The misalignment between the Pt electron density and photocatalytic activity infers that the electron donation originated from the Schottky junction is not the sole factor determining the activity.

Therefore, the electron transfer from Pt interband excitation under light irradiation, which has been reported to exert influence on photocatalysis,[22] might not be ignorable. The Schottky barrier will be formed at the interface between the MOF and Pt NPs once the occurrence of their contact. The height of Schottky barrier is related to the work function of the metal and the electron affinity of the semiconductor analog, i.e. the MOFs (Figure 5b).[9b,23] Under light irradiation, the electrons with high energy by Pt interband excitation would possibly overcome Schottky barrier and be injected into the MOFs. As shown in Table S8, the Schottky barrier height can be calculated by analyzing the work function of Pt and electron affinity of the MOFs. In opposition to the LUMO levels of the MOFs, the Schottky barrier heights follow the order of Pt/ZIF-8 > Pt/MIL-125 > Pt/UiO-66. Results indicate that the Pt interband electrons excited by 450 nm light irradiation can jump over the Schottky barrier in Pt/UiO-66 and Pt/MIL-125 rather than Pt/ZIF-8, the latter of which requires $\leq$430 nm light irradiation with higher energy (Figure 5c). When the higher energy of 405 nm light irradiation is adopted, the electrons from Pt interband excitation can be injected to ZIF-8. As a result, the apparent quantum yield (AQY) is much lower at 405 nm than that at 450 nm light irradiation, demonstrating the Pt electron injection is detrimental to the photocatalytic activity (Figure S30). EPR measurements for Pt/UiO-66 and Pt/MIL-125 further manifest the electron injection mechanism, where the enhanced single electron signals upon light irradiation (>420 nm) suggest the hot electron injection from Pt interband excitation to the MOFs (Figure S31). Notably, although there is no electron injection from Pt to SiO_2, the activity of Pt/SiO_2 is much lower than ZIF-8, reflecting that the electron donation from ZIF-8 to Pt in the first step (upon contact) also plays a significant role in the activity.

The above analyses and results demonstrate that the photocatalytic oxidation over the Pt/MOFs is governed by the combination of the MOF electron donation and Pt interband excitation. The detailed electron transfer between the MOFs and Pt is illustrated (Figure 5d–f). Firstly, the Fermi level difference between Pt and the MOFs drives electron flow from the MOFs to Pt NPs to align their Fermi levels, giving rise to the electron donation effect from the MOFs to Pt.[24] Relative to Pt/ZIF-8, the LUMO levels of both UiO-66 and MIL-125 are closer to the Fermi level of Pt, giving rise to the less electron donation from the MOFs in Pt/UiO-66 and Pt/MIL-125 (Figure 5d). Upon the equilibrium establishment of Fermi level, the Schottky barriers with different heights will be constructed at the interface of Pt and the MOFs (Figure 5e). When introducing light irradiation, Pt interband excitation occurs, during which the excited electrons would possibly jump over Schottky junction to be injected back into the MOFs (dependent on the photon and electron energy) or participate in the photocatalytic reaction (O_2 activation) (Figure 5f). Given that the reverse injection of electrons from Pt interband excitation is easier in Pt/UiO-66 and Pt/MIL-125 than that in Pt/ZIF-8 with the higher energy gap, the electron destination from Pt interband excitation under 450 nm light irradiation in the Pt/MOFs is different. The electrons cannot be injected into the MOF but only activate O_2 in Pt/ZIF-8; by contrast, they not only go to the LUMO of the MOFs but also activate O_2 in Pt/UiO-66 and Pt/MIL-125. The lowest charge

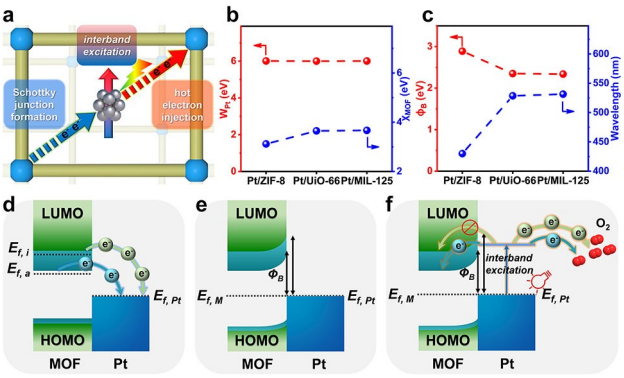

Figure 5. a) Schematic illustration of electron transfer pathways in Pt/MOF. b) Work function of Pt (denoted W_{Pt}) and electron affinity of the MOFs (denoted χ_{MOF}) in the Pt/MOF. c) Schottky junction height (denoted Φ_B) and wavelength of light acquired to overcome the Schottky junction for Pt/MOFs. d), e) Schematic illustration of band diagrams for the Pt/MOF, showing d) the formation of Schottky junction with electron transfer from the MOF to Pt by contact, following by e) equilibrium establishment with Fermi energy shift, and then f) the migration of electrons originated from interband excitation of Pt NPs under light irradiation. The MOF band diagrams are shown as two parts: green parts denote inert support (ZIF-8) and cyan parts denote active support (UiO-66 or MIL-125). For the electron transfer pathway in Pt/MOF, the color is in line with that of the corresponding MOF band diagram. The Fermi level $E_{f,\ inert\ support}$, $E_{f,\ active\ support}$ and $E_{f,\ MOF}$ are shortened to be E_{fi}, E_{fa} and E_{fM}.

separation efficiency of Pt/ZIF-8 among all the photocatalysts, as evidenced by the photocurrent response and electrochemical impedance spectroscopy (EIS) results (Figure S32), well supports the above explanation. Overall, the electron donation from the MOFs to Pt and the electrons from Pt interband excitation possibly to the MOFs, in reversed electron transfer, can synergistically modulate the Pt electron density. As a result, not only more electron donation in the first process but also more electrons for O_2 activation in the other process are available in Pt/ZIF-8, which explains the uncommon advantage of supporting Pt with an inert ZIF-8, accounting for the significantly higher photocatalytic oxidation performance than the corresponding counterparts.

Conclusion

In summary, the non-reducible support has been uncommonly observed to be more favorable to reducible counterparts toward promoting photocatalysis. Specifically, Pt NPs are supported by three representative MOFs (ZIF-8, UiO-66 and MIL-125) for photocatalytic oxidative coupling of benzylamines. Despite the similar Pt sizes and loading amounts, Pt/ZIF-8 exhibits excellent activity, far surpassing that of Pt/UiO-66 and Pt/MIL-125. Both XPS and CO-DRIFT spectra demonstrate that the electron donation from different MOFs to Pt driven by the formation of the Schottky junction is distinct, affecting the Pt electron density. Upon 450 nm light irradiation, the electrons from Pt interband excitation are reversely injected into the MOF, which is allowed in Pt/UiO-66 and Pt/MIL-125, while forbidden in Pt/ZIF-8 due to the higher energy gap of the latter. The higher Pt electron density in Pt/ZIF-8 induced by the above two processes contributes to its stronger capability to generate $O_2^{\bullet-}$, which is responsible for its superior activity to Pt/UiO-66 and Pt/MIL-125. This work demonstrates the unusual advantages of metal nanoparticulate catalysts with redox-inert supports in photocatalysis, and enriches our understanding of promoting photocatalysis by modulating metal–support interactions, including non-reducible supports.

Acknowledgements

This work was supported by the National Key Research and Development Program of China (2021YFA1500402), the National Natural Science Foundation of China (21725101, 21871244, 22161142001, and 22101269), International Partnership Program of CAS (211134KYSB20190109) and Collaborative Innovation Program of Hefei Science Center, CAS (2020HSC-CIP005).

Conflict of Interest

The authors declare no conflict of interest.

Data Availability Statement

The data that support the findings of this study are available from the corresponding author upon reasonable request.

Keywords: Metal–Organic Frameworks · Metal–Support Interactions · Non-Reducible Supports · Photocatalysis · Supported Catalysts

[1] a) M. Cargnello, J. J. D. Jaén, J. C. H. Garrido, K. Bakhmutsky, T. Montini, J. J. C. Gámez, R. J. Gorte, P. Fornasiero, *Science* **2012**, *337*, 713–717; b) S. Kattel, P. J. Ramírez, J. G. Chen, J. A. Rodriguez, P. Liu, *Science* **2017**, *355*, 1296–1299; c) J. Zhang, L. Wang, B. Zhang, H. Zhao, U. Kolb, Y. Zhu, L. Liu, Y. Han, G. Wang, C. Wang, D. S. Su, B. C. Gates, F.-S. Xiao, *Nat. Catal.* **2018**, *1*, 540–546.

[2] a) Z. Jin, M. Xiao, Z. Bao, P. Wang, J. Wang, *Angew. Chem. Int. Ed.* **2012**, *51*, 6406–6410; *Angew. Chem.* **2012**, *124*, 6512–6516; b) X.-H. Li, M. Antonietti, *Chem. Soc. Rev.* **2013**, *42*, 6593–6604; c) Q.-L. Zhu, Q. Xu, *Chem* **2016**, *1*, 220–245; d) N. Wang, Q. Sun, J. Yu, *Adv. Mater.* **2019**, *31*, 1803966; e) Y. Wang, C. Wang, L. Wang, L. Wang, F.-S. Xiao, *Acc. Chem. Res.* **2021**, *54*, 2579–2590.

[3] a) J. Lu, B. Fu, M. C. Kung, G. Xiao, J. W. Elam, H. H. Kung, P. C. Stair, *Science* **2012**, *335*, 1205–1208; b) N. Ta, J. J. Liu, S. Chenna, P. A. Crozier, Y. Li, A. Chen, W. Shen, *J. Am. Chem. Soc.* **2012**, *134*, 20585–20588; c) W. Karim, C. Spreafico, A. Kleibert, J. Gobrecht, J. VandeVondele, Y. Ekinci, J. A. van Bokhoven, *Nature* **2017**, *541*, 68–71; d) T. Komanoya, T. Kinemura, Y. Kita, K. Kamata, M. Hara, *J. Am. Chem. Soc.* **2017**, *139*, 11493–11499; e) P. Liu, R. Qin, G. Fu, N. Zheng, *J. Am. Chem. Soc.* **2017**, *139*, 2122–2131; f) J. Huang, S. He, J. L. Goodsell, J. R. Mulcahy, W. Guo, A. Angerhofer, W. D. Wei, *J. Am. Chem. Soc.* **2020**, *142*, 6456–6460.

[4] a) G. Kennedy, L. R. Baker, G. A. Somorjai, *Angew. Chem. Int. Ed.* **2014**, *53*, 3405–3408; *Angew. Chem.* **2014**, *126*, 3473–3476; b) C. Hernandez Mejia, T. W. van Deelen, K. P. de Jong, *Nat. Commun.* **2018**, *9*, 4459.

[5] a) L. Liu, X. Zhang, L. Yang, L. Ren, D. Wang, J. Ye, *Natl. Sci. Rev.* **2017**, *4*, 761–780; b) C. Dong, C. Lian, S. Hu, Z. Deng, J. Gong, M. Li, H. Liu, M. Xing, J. Zhang, *Nat. Commun.* **2018**, *9*, 1252; c) E. Peiris, S. Sarina, E. R. Waclawik, G. A. Ayoko, P. Han, J. Jia, H.-Y. Zhu, *Angew. Chem. Int. Ed.* **2019**, *58*, 12032–12036; *Angew. Chem.* **2019**, *131*, 12160–12164; d) Y. Gao, W. Nie, Q. Zhu, X. Wang, S. Wang, F. Fan, C. Li, *Angew. Chem. Int. Ed.* **2020**, *59*, 18218–18223; *Angew. Chem.* **2020**, *132*, 18375–18380; e) L. Lin, Z. Lin, J. Zhang, X. Cai, W. Lin, Z. Yu, X. Wang, *Nat. Catal.* **2020**, *3*, 649–655.

[6] S. Mukherjee, L. Zhou, A. M. Goodman, N. Large, C. Ayala-Orozco, Y. Zhang, P. Nordlander, N. J. Halas, *J. Am. Chem. Soc.* **2014**, *136*, 64–67.

[7] a) H. Furukawa, K. E. Cordova, M. O'Keeffe, O. M. Yaghi, *Science* **2013**, *341*, 1230444; b) H.-C. Zhou, S. Kitagawa, *Chem. Soc. Rev.* **2014**, *43*, 5415–5418; c) T. Islamoglu, S. Goswami, Z. Li, A. J. Howarth, O. K. Farha, J. T. Hupp, *Acc. Chem. Res.* **2017**, *50*, 805–813; d) H. Li, L. Li, R.-B. Lin, W. Zhou, Z. Zhang, S. Xiang, B. Chen, *EnergyChem* **2019**, *1*, 100006; e) J. Nyakuchena, S. Ostresh, D. Streater, B. Pattengale, J. Neu, C. Fiankor, W. Hu, E. D. Kinigstein, J. Zhang, X. Zhang, C. A. Schmuttenmaer, J. Huang, *J. Am. Chem. Soc.* **2020**, *142*, 21050–21058; f) L. Jiao, J. Wang, H.-L. Jiang, *Acc. Mater. Res.* **2021**, *2*, 327–339.

[8] a) A. Aijaz, A. Karkamkar, Y. J. Choi, N. Tsumori, E. Ronnebro, T. Autrey, H. Shioyama, Q. Xu, *J. Am. Chem. Soc.* **2012**, *134*, 13926–13929; b) X. Li, T. W. Goh, L. Li, C. Xiao, Z.

Guo, X. C. Zeng, W. Huang, *ACS Catal.* **2016**, *6*, 3461–3468; c) Q. Yang, Q. Xu, H.-L. Jiang, *Chem. Soc. Rev.* **2017**, *46*, 4774–4808; d) G. Li, S. Zhao, Y. Zhang, Z. Tang, *Adv. Mater.* **2018**, *30*, 1800702; e) F. Chen, K. Shen, J. Chen, X. Yang, J. Cui, Y. Li, *ACS Cent. Sci.* **2019**, *5*, 176–185; f) C. Fang, L. Liu, J. Weng, S. Zhang, X. Zhang, Z. Ren, Y. Shen, F. Meng, B. Zheng, S. Li, J. Wu, W. Shi, S. Lee, W. Zhang, F. Huo, *Angew. Chem. Int. Ed.* **2021**, *60*, 976–982; *Angew. Chem.* **2021**, *133*, 989–995; g) L. Li, Z. Li, W. Yang, Y. Huang, G. Huang, Q. Guan, Y. Dong, J. Lu, S.-H. Yu, H.-L. Jiang, *Chem* **2021**, *7*, 686–698.

[9] a) M. Usman, S. Mendiratta, K. L. Lu, *Adv. Mater.* **2017**, *29*, 1605071; b) J.-D. Xiao, L. Han, J. Luo, S.-H. Yu, H.-L. Jiang, *Angew. Chem. Int. Ed.* **2018**, *57*, 1103–1107; *Angew. Chem.* **2018**, *130*, 1115–1119; c) N. Kolobov, M. G. Goesten, J. Gascon, *Angew. Chem. Int. Ed.* **2021**, *60*, 26038–26052; *Angew. Chem.* **2021**, *133*, 26242–26256; d) E.-X. Chen, M. Qiu, Y.-F. Zhang, L. He, Y.-Y. Sun, H.-L. Zheng, X. Wu, J. Zhang, Q. Lin, *Angew. Chem. Int. Ed.* **2022**, *61*, e202111622; *Angew. Chem.* **2022**, *134*, e202111622.

[10] a) B. Hammer, J. K. Nørskov, *Nature* **1995**, *376*, 238–240; b) J. K. Nørskov, T. Bligaard, B. Hvolbaek, F. Abild-Pedersen, I. Chorkendorff, C. H. Christensen, *Chem. Soc. Rev.* **2008**, *37*, 2163–2171.

[11] a) S. Sarina, H.-Y. Zhu, Q. Xiao, E. Jaatinen, J. Jia, Y. Huang, Z. Zheng, H. Wu, *Angew. Chem. Int. Ed.* **2014**, *53*, 2935–2940; *Angew. Chem.* **2014**, *126*, 2979–2984; b) U. Aslam, V. G. Rao, S. Chavez, S. Linic, *Nat. Catal.* **2018**, *1*, 656–665.

[12] a) J. Zhao, S. C. Nguyen, R. Ye, B. Ye, H. Weller, G. A. Somorjai, A. P. Alivisatos, F. D. Toste, *ACS Cent. Sci.* **2017**, *3*, 482–488; b) J. Li, Q. Shen, J. Li, J. Liang, K. Wang, X.-H. Xia, *J. Phys. Chem. Lett.* **2020**, *11*, 8322–8328; c) W. Wang, J. Fang, X. Huang, *Appl. Surf. Sci.* **2020**, *513*, 145830; d) P. Lyu, R. Espinoza, M. I. Khan, W. C. Spaller, S. Ghosh, S. C. Nguyen, *iScience* **2022**, *25*, 103737.

[13] a) K. S. Park, Z. Ni, A. P. Côté, J. Y. Choi, R. Huang, F. J. Uribe-Romo, H. K. Chae, M. O'Keeffe, O. M. Yaghi, *Proc. Natl. Acad. Sci. USA* **2006**, *103*, 10186–10191; b) X.-C. Huang, Y.-Y. Lin, J.-P. Zhang, X.-M. Chen, *Angew. Chem. Int. Ed.* **2006**, *45*, 1557–1559; *Angew. Chem.* **2006**, *118*, 1587–1589; c) J. H. Cavka, S. Jakobsen, U. Olsbye, N. Guillou, C. Lamberti, S. Bordiga, K. P. Lillerud, *J. Am. Chem. Soc.* **2008**, *130*, 13850–13851; d) M. Dan-Hardi, C. Serre, T. Frot, L. Rozes, G. Maurin, C. Sanchez, G. Ferey, *J. Am. Chem. Soc.* **2009**, *131*, 10857–10859.

[14] a) A. Pinchuk, G. v Plessen, U. Kreibig, *J. Phys. D* **2004**, *37*, 3133–3139; b) T. Pakizeh, *J. Opt.* **2013**, *15*, 025001.

[15] H.-Q. Xu, J. Hu, D. Wang, Z. Li, Q. Zhang, Y. Luo, S.-H. Yu, H.-L. Jiang, *J. Am. Chem. Soc.* **2015**, *137*, 13440–13443.

[16] Y.-Y. Cai, X.-H. Li, Y.-N. Zhang, X. Wei, K.-X. Wang, J.-S. Chen, *Angew. Chem. Int. Ed.* **2013**, *52*, 11822–11825; *Angew. Chem.* **2013**, *125*, 12038–12041.

[17] a) S. K. Cushing, J. Li, F. Meng, T. R. Senty, S. Suri, M. Zhi, M. Li, A. D. Bristow, N. Wu, *J. Am. Chem. Soc.* **2012**, *134*, 15033–15041; b) K. Bi, M. Bi, Y. Hao, W. Luo, Z. Cai, X. Wang, Y. Huang, *Nano Energy* **2018**, *51*, 513–523.

[18] M. T. Schümperli, C. Hammond, I. Hermans, *ACS Catal.* **2012**, *2*, 1108–1117.

[19] Q. Xiao, S. Sarina, E. R. Waclawik, J. Jia, J. Chang, J. D. Riches, H. Wu, Z. Zheng, H.-Y. Zhu, *ACS Catal.* **2016**, *6*, 1744–1753.

[20] a) Y. Kakuma, A. Y. Nosaka, Y. Nosaka, *Phys. Chem. Chem. Phys.* **2015**, *17*, 18691–18698; b) Y.-Q. Huang, H.-J. Song, Y. X. Liu, Q.-M. Wang, *Chem. Eur. J.* **2018**, *24*, 2065–2069.

[21] a) C. Xu, H. Liu, D. Li, J.-H. Su, H.-L. Jiang, *Chem. Sci.* **2018**, *9*, 3152–3158; b) S. Swaminathan, V. G. Rao, J. K. Bera, M. Chandra, *Angew. Chem. Int. Ed.* **2021**, *60*, 12532–12538; *Angew. Chem.* **2021**, *133*, 12640–12646.

[22] H. Sakamoto, T. Ohara, N. Yasumoto, Y. Shiraishi, S. Ichikawa, S. Tanaka, T. Hirai, *J. Am. Chem. Soc.* **2015**, *137*, 9324–9332.

[23] a) S. Bai, J. Jiang, Q. Zhang, Y. Xiong, *Chem. Soc. Rev.* **2015**, *44*, 2893–2939; b) M. R. Khan, T. W. Chuan, A. Yousuf, M. N. K. Chowdhury, C. K. Cheng, *Catal. Sci. Technol.* **2015**, *5*, 2522–2531.

[24] a) J. Bardeen, *Phys. Rev.* **1947**, *71*, 717–727; b) R. H. Williams, *Contemp. Phys.* **1982**, *23*, 329–351; c) L. Pei, T. Li, Y. Yuan, T. Yang, J. Zhong, Z. Ji, S. Yan, Z. Zou, *Chem. Commun.* **2019**, *55*, 11754–11757.

Manuscript received: April 26, 2022
Accepted manuscript online: June 6, 2022
Version of record online: June 24, 2022